A Novel Photometric Method for Real-Time 3D Reconstruction of Fingerprint

Wuyuan Xie[1,2], Zhan Song[1,2], and Xiaoting Zhang[1,2]

[1] Shenzhen Institutes of Advanced Technology, Chinese Academy of Sciences, China
[2] The Chinese University of Hong Kong, Hong Kong, China
{wy.xie,zhan.song,xt.zhang}@sub.siat.ac.cn

Abstract. 3D fingerprint recognition is an emerging technology in biometrics. However, current 3D fingerprint acquisition systems are usually with complex structure and high-cost and that has become the main obstacle for its popularization. In this work, we present a novel photometric method and an experimental setup for real-time 3D fingerprint reconstruction. The proposed system consists of seven LED lights that mounted around one camera. In the surface reflectance modeling of finger surface, a simplified Hanrahan-Krueger model is introduced. And a neural network approach is used to solve the model for accurate estimation of surface normals. A calibration method is also proposed to determine the lighting directions as well as the correction of the lighting fields. Moreover, to stand out the fingerprint ridge features and get better visual effects, a linear transformation is applied to the recovered normals field. Experiments on live fingerprint and the comparison with traditional photometric stereo algorithm are used to demonstrate its high performance.

1 Introduction

Fingerprint recognition has been a classical topic in computer vision community over last decades. Current fingerprint system usually consists of an image sensor, a light source and a touch panel, and the recognition task is performed over the captured 2D fingerprint image. In practice, the imaged fingerprint is usually degraded caused by improper finger placement, skin deformation, slippage, smearing of finger and touch panel surface [1] etc. Moreover, the touching fingerprint collection method also causes the problem of disease propagation. To overcome these drawbacks, a technique named touch-less fingerprint recognition systems is emerging recently. Such systems can obtain the 3D model of the finger surface by employing a 3D scanning procedure. In comparison with traditional 2D fingerprint system, the 3D system can outperform in both recognition rate and operation efficiency [2-3].

The touch-less live fingerprints acquisition is essentially a problem of 3D surface reconstruction. And methods used for this end are nothing more than those common reconstruction methods in computer vision like Structured Light System (SLS), stereo vision and Shape from Silhouette etc. As a frontier technology, there still few works have been reported in this domain. In [2], an experimental system which consists of five cameras and sixteen green LED lights is proposed. The fingerprint images under

G. Bebis et al. (Eds.): ISVC 2010, Part II, LNCS 6454, pp. 31–40, 2010.

various illuminations are captured by the cameras. Corresponding silhouettes are extracted from these images and then are used for the 3D modelling of the finger surface via Shape from Silhouette method. In [3], a structured light system is proposed for the 3D reconstruction of fingerprint. The system contains a projection device and a synchronized camera. By projecting a sequence of strip patterns onto the finger surface and imaged by the camera, 3D model of the fingerprint can be achieved in less than one second. The two systems have been demonstrated to be effective for quick 3D fingerprint acquisition and outperform current 2D systems in recognition rates. However, the main obstacle for present 3D fingerprint technologies to replace 2D systems comes from their complex structure and high cost. More portable and low-cost devices for quick 3D acquisition of fingerprint are urgently demanded.

In this paper, a novel touch-less 3D fingerprint acquisition system that based upon the principle of Photometric Stereo (PS) is proposed. The system consists of only one camera and seven LED lamps. In the PS methods, its performance highly depends on the surface reflectance modeling as well as the lighting conditions. With a brief analysis and comparison of some present human skin reflectance models, the more reasonable Hanrahan-Krueger (HK) [4] model is used and simplified in our work. A novel method for the calibration of the LED lights including the light direction and correction of the lighting field is proposed. Finally, a surface normal transformation procedure is applied to boost the fingerprints details like the surface ridge features.

The paper is organized as follows. In Section 2, we briefly analyze the rationality of the simplified HK model as well as the solution of the model parameters. In Section 3, system calibration and the surface normal transformation methods are presented. Experimental results on a platicine toy, palm and live fingerprints are offered in Section 4. Conclusion and future work can be found in Section 5.

2 Reflectance Property Modeling of the Finger Surface

Traditional PS methods are usually based on the assumption of Lambert reflection law [5-8], i.e., the target surfaces are supposed with ideal diffuse reflection. Given three or more lights with known directions, surface normal at any image point can be calculated by solving a group of linear Lambertion equations. As for human skin, it is more close to a kind of translucent material whose reflectance model contains certain multiple scattering and specular reflections. And thus makes traditional PS method incapable to get precise 3D reconstruction result. To model the human skin more precisely, Georghiades [9] has introduced a non-Lambertian reflectance model, the Torrance and Sparrow (TS) model, into an uncalibrated PS method to calculate reflectance parameters of human skin and to reduce the negative effects of generalized bas-relief (GBR) [10]. TS model is a physically-based model which assumes that the skin reflectance consists of two components: a) Lambertian lobe at a particular position on the skin and b) purely surface scattering component. In comparison, Hanrahan-Krueger (HK) is such a model for subsurface scattering in layered surfaces based on one dimensional linear transport theory. The basic idea is that the amount of light reflected by a material that exhibits subsurface scattering is calculated by summing

the amount of light reflected by each layer times the percentage of light that actually reaches that layer. In the algorithm, skin is modeled as a two-layer material which is consist of epidermis and dermis, and each layer has different reflectance parameters that determine how light reflect from that layer as shown in Fig. 1. Therefore it's a more reasonable model for translucent surfaces like human skin and fingers.

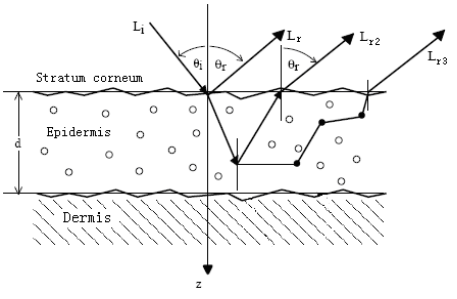

Fig. 1. Reflection and multiple scattering in the two-layer HK skin model

In the original HK model, each layer is parameterized by the absorption cross section σ_a, scattering cross section σ_s, layer thickness d, and the mean cosine g of the phase function. And p determines in which direction the light is likely to scatter as (1), where ϕ is the angle between the light and the view directions:

$$p(\phi, g) = \frac{1}{4\pi} \cdot \frac{1-g^2}{4\pi(1+g^2-2g\cos\phi)^{2/3}} \tag{1}$$

The total cross section σ_t, optical depth τ_d and albedo ζ can be expressed as:

$$\sigma_t = \sigma_s + \sigma_a,\ \tau_d = \sigma_t \cdot d,\ \zeta = \sigma_s / \sigma_t \tag{2}$$

where σ_t represents the expected number of either absorptions or scatterings per unit length. The optical depth is used to determine how much light is attenuated from the top to the bottom of the layer. ζ indicates the percentage of interactions that result in scattering. More details about HK model discussion can be found in [4].

In this work, to simplify the HK model, a Lambertion term L_m is used to approximate the multiple scattering $L_{r2}, L_{r3}, \cdots, L_{rm}$ as:

$$L_m = L_{r2} + L_{r3} + \cdots + L_{rm} = \rho\cos\theta_i \tag{3}$$

where ρ is an defined albedo, which determines the amount of diffuse light caused by multiple scattering, and θ_i is the incidence angle between the normal vector and the light direction. Then the revised HK model can be written as:

$$L_r(\theta_r, \varphi_r) = \zeta T^{12} T^{21} p(\phi, g) \frac{\cos\theta_i}{\cos\theta_i + \cos\theta_r} (1 - e^{-\tau_d (\frac{1}{\cos\theta_i} + \frac{1}{\cos\theta_r})}) L_i(\theta_i, \varphi_i) + L_m$$

where T^{12} and T^{21} refer to the Fresnel transmittance terms for lights entering and leaving the surface respectively, and are assumed to be constant over the whole surface as well as g. By replacing $p(\phi, g)$, (ζ, τ_d) and L_m with the right side of Eqn.(1), Eqn.(2), and Eqn.(3) respectively, the simplified HK model can be expressed as:

$$L_r = \frac{\delta_s}{\delta_t} T^{12} T^{21} \frac{(1-g)^2 \cos\theta_i (1 - e^{-(\delta_t d)(\frac{\cos\theta_r + \cos\theta_i}{\cos\theta_r \cos\theta_i})}) L_i}{16\pi^2 (1 + g^2 - 2g\cos\phi)^{2/3} (\cos\theta_i + \cos\theta_r)} + \rho \cos\theta_i \tag{4}$$

Given any incident light $L_i(\theta_i, \varphi_i)$ with incident angle (θ_i, φ_i), the reflection light $L_r(\theta_r, \varphi_r)$ can be calculated through Eqn. (4). Eqn. (4) is only calculated for epidermis. Mostly, scattering in the dermis layer will do minor contributions to the final fingerprint image. As a result, in our model, parameters in this layer are ignored and thus also benefit the whole computation cost.

To solve the surface normal vector $\mathbf{n} = (n_x, n_y, n_z)$, $\cos\theta_i$, $\cos\phi$ and $\cos\theta_r$, Eqn. (4) can be rewritten in the form of $\mathbf{n}$'s inner product between lighting direction $\mathbf{l} = (l_x, l_y, l_z)$ and the view direction $\mathbf{z} = (z_x, z_y, z_z)$ as:

$$\cos\theta_i = \mathbf{l} \cdot \mathbf{n},\ \cos\theta_r = \mathbf{z} \cdot \mathbf{n},\ \cos\phi = \mathbf{l} \cdot \mathbf{z} \tag{5}$$

There are ten unknowns i.e. $n_x, n_y, n_z, \rho, d, \sigma_s, \sigma_a, g, T^{12}$ and T^{21} in Eqn. (4). Notice that each surface point is associated with a unique quadruple $(\theta_i, \varphi_i; \theta_r, \varphi_r)$. To clarify the statements, two superscripts are used to mark those point-unique parameters with the first refers to the order of the surface point and the second one indicates the number of light source. For example, $L_r^{j,k}$ represents $L_r(\theta_r, \varphi_r)$ of the j^{th} surface point under illumination of the k^{th} light, $\mathbf{n}^j$ refers to normal vector of the j^{th} surface point, while $\mathbf{l}^k$ represents the direction vector of the k^{th} light. Then we can formulate the simultaneous recovery to the following nonlinear optimization problem:

$$\arg \min_{\mathbf{x}} E(\mathbf{x}),\ \text{where}\ \ E(\mathbf{x}) = \sum_{j,k} (L_r^{j,k} - I^{j,k})^2 \tag{6}$$

where $I^{j,k}$ represents the pixel intensity on the k^{th} image of the j^{th} surface point, and $\mathbf{x}$ is a vector containing all the unknown parameters to be estimated, i.e.,

$$\mathbf{x} = (n_x^j, n_y^j, n_z^j, \rho^j, d^j, \sigma_s^j, \sigma_a^j, g, T^{12}, T^{21}), \{\mathbf{x} \in \mathbf{R}^n\}$$

To solve $\mathbf{x}$ from Eqn. (6), a neural network algorithm named ZCNK is used in this work. As described in [11], the object function can be written as:

$$F(\mathbf{x}) = \partial E / \partial \mathbf{x} \tag{7}$$

Since $\mathbf{x}$ is an *n*-dimensional vector, $F(\mathbf{x})$ consists of *n* equations. Unlike the initialization method in [11] which takes optional values for all components of $\mathbf{x}$, we initialize $\mathbf{x}$ as following way:

(a) For $\mathbf{n}^j$ *and* ρ^j *, their initial values are calculated from Equation (3) through the least square method;*

(b) For $d^j, \sigma_s^j, \sigma_a^j,$ and g *, we refer to [4] for their initial values;*

(c) T^{12} and T^{21} *are initialized randomly;*

3 System Calibration and 3D Recovery

3.1 Calibration of Lighting Directions

To determine incident light angles of all the lights, a method proposed in [12] is used. In [12], two cameras and a shiny ball without position and radius information are used to calibrate the lighting directions. Since just one camera is used in our system, the lighting directions are calibrated by the use of one camera and a shiny ball with known radius r. Focal length f and principle point C of the camera can be obtained via method mentioned in [13]. With reference to the camera coordinate frame, each lighting direction can be represented as $\mathbf{l} = (lx, ly, lz)$ as shown in Fig. 2(a). According to [12], the radius d_i can be expressed as:

$$d_i^2 = |CS|^2 - \cos^2\theta = h_i(s_x, s_y, s_z), \ \cos\theta = \frac{(CS \cdot CB_i)}{|CS||CB_i|} = \frac{\sqrt{|CS|^2 - d_i^2}}{|CS|} \tag{8}$$

where B_i is a boundary point on the image plane with a checked position (i_1, j_1, f), then Eqn. (8) contains only three unknowns, i.e. center of the sphere $S = (s_x, s_y, s_z)$. Suppose there are *m* boundary points $B_i, i \in (1, \ldots, m)$ obtained by edge detection algorithm [14], then an error function can be defined as:

$$EOF = \sum_{i=1}^{m} (h_i - r^2)^2 \tag{9}$$

Minimizing this error function gives us three equations about S, from which the optimal values of the sphere location can be solved. Notice that specular point $P(i_1, j_1)$ on the image plane can be easily detected by finding the brightest image point. Once S is obtained, the corresponding point S_1 of p on the surface and the surface normal vector $\mathbf{N}$ on S_1, as illustrated in Fig. 2(b), can be solved as:

$$\mathbf{l} = 2(\mathbf{N} \cdot \mathbf{R})\mathbf{N} - \mathbf{R} \tag{10}$$

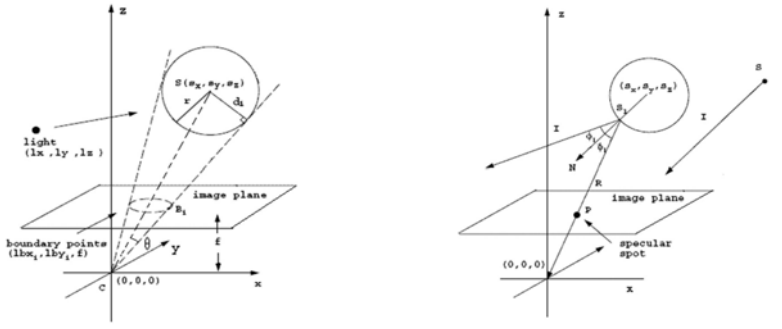

(a) (b)

Fig. 2. (a) Illustration of light direction calibration. (b) Relation of **N**, **R**, and **l**.

3.2 Correction of Lighting Field

Since lighting fields of these LED lamps are usually not uniformly distributed as shown in Fig. 3(a). Notice that when the light position is fixed, the brightest spot has a fixed area. This means that under the illumination of a fixed LED, to any image point at (i, j) , the portion $p(i, j)$ of its intensity value $I(i, j)$ to the brightest pixel value $I_{\max}$ is constant no matter what kind of the shape of the object is, i.e.,

$$p(i, j) = I(i, j) / I_{\max} \tag{11}$$

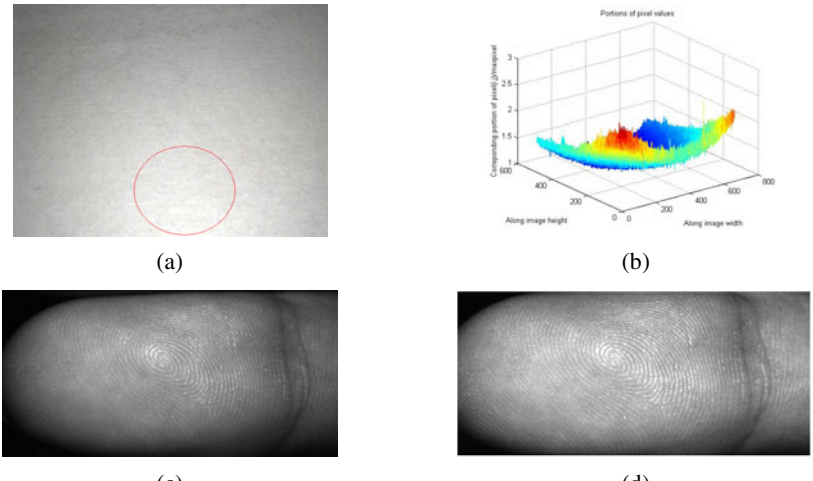

(a) (b)

(c) (d)

Fig. 3. (a) A white paper is used to correct the LED lighting field so as to make the luminance distribution more uniform. (b) The diagram of values of p that calculated from (a). (c) Original image without calibration. (d) Result after lighting field correction.

Fig. 3(b) gives the diagram of values of p that calculated from Fig. 3(a). With above procedure, the resulting image can have the same illumination at all image points under l^k. Fig. 3(c) and (d) give the comparison between the original image and the corrected image with the proposed method.

3.3 Linear Transformation of the Normal Field

Once surface normal vector $\mathbf{n}$ has been estimated, a linear normal transformation method [7] is adopted consequently. In the algorithm, the average of normal vectors over a local patch w is calculated as a local reference, and the difference between the original surface normal and this reference vector can be amplified as:

$$\mathbf{n}' = \mathbf{n} + k(\mathbf{n} - normalize(\sum_{j=1}^{w} \mathbf{n}_j)) \tag{12}$$

This procedure aims to amplify the angle between two neighboring normal vectors and thus improve the visual effect and contrast of the reconstructed 3D model especially to the fingerprint ridges.

4 Experimental Results

Our experimental system consists of a camera with resolution of 659×493 pixels and seven LED lamps mounted around it as shown in Fig. 4. An external I/O board is developed to synchronize the camera and LED lamps. The whole capturing time can be controlled within 0.2 s. Each lamp is connected with a metallic hose so that its illuminant angle can be adjusted freely to fit the size of the target object.

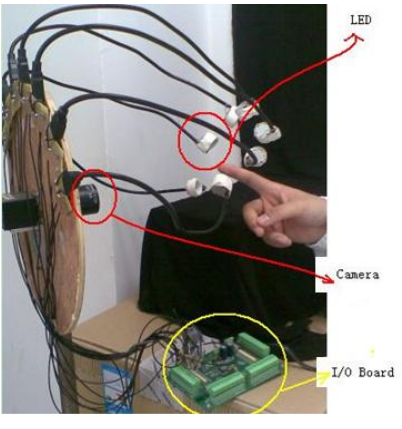

Fig. 4. The experimental system consists of a camera and seven LED lamps and they are synchronized via an external I/O board

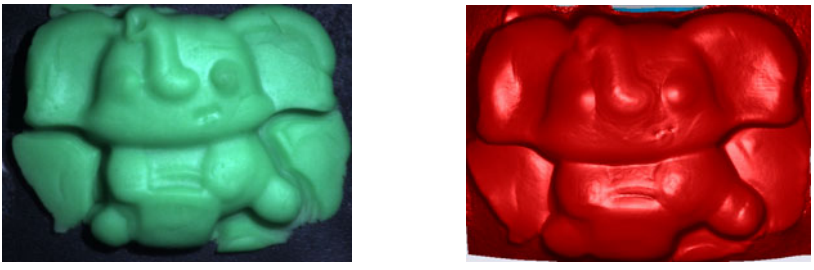

(a) (b)

Fig. 5. Reconstruction of a plasticine toy with translucent surface

In the experiment with a plasticine toy as shown in Fig. 5, the parameters $d^j, \sigma_s^j, \sigma_a^j$ and g are set to 0.085 mm, 50 mm^{-1}, 3.8 mm^{-1} and 0.79 respectively.

In the experiment with human palm and fingerprint, the four parameters are set to 0.12 mm, 30 mm^{-1}, 4.5 mm^{-1} and 0.81 respectively. Fig. 6(a) shows the original image of human palm image under one LED illumination. The reconstruction result without normal transformation is as shown in Fig. 6(b). The result looks smooth with palm print almost invisible. After the transformation (w and k in Eqn. (8) are set to 7

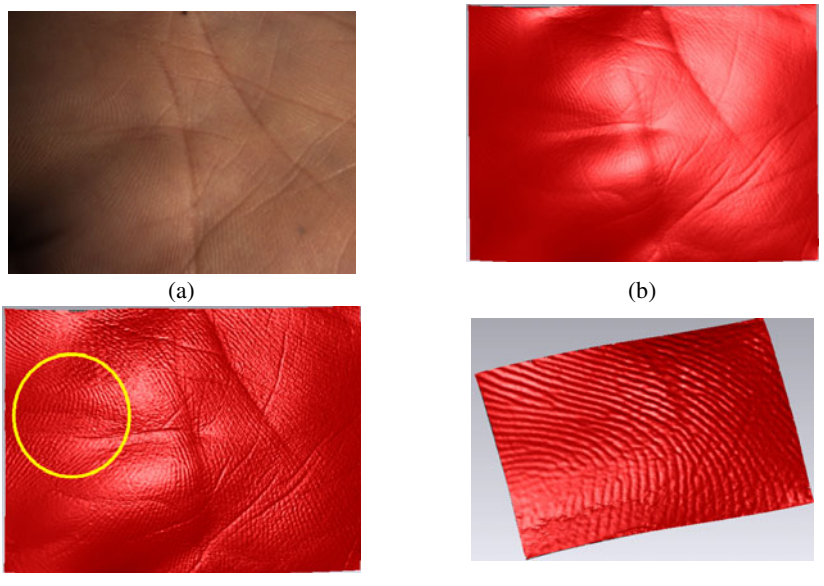

(a) (b)

(c) (d)

Fig. 6. 3D reconstruction of palm print. (a) Original palm image under one LED illumination. (b) The reconstructed 3D model of palm print without surface normal transformation. (c) 3D model with normal transformation. (d) Cropped 3D image for close observation.

and 2.5 respectively), palm print can be discovered more visually as shown Fig. 6(c). One cropped area is enlarged in Fig. 6(d) for close observation.

The last experiment is conducted on a live finger as shown in Fig. 7(a). The result by traditional Lambert model is also presented for comparison. From Fig. 7(b), we can see that Lambert model fails to obtain skeletons of the fingerprint in the margins. It is mainly caused by that in Lambertion reflection model, pixel brightness is supposed to be independent on viewing direction. But it is not true for finger surface, and therefore makes the recovered surface normal inaccurate as well as 3D shape.

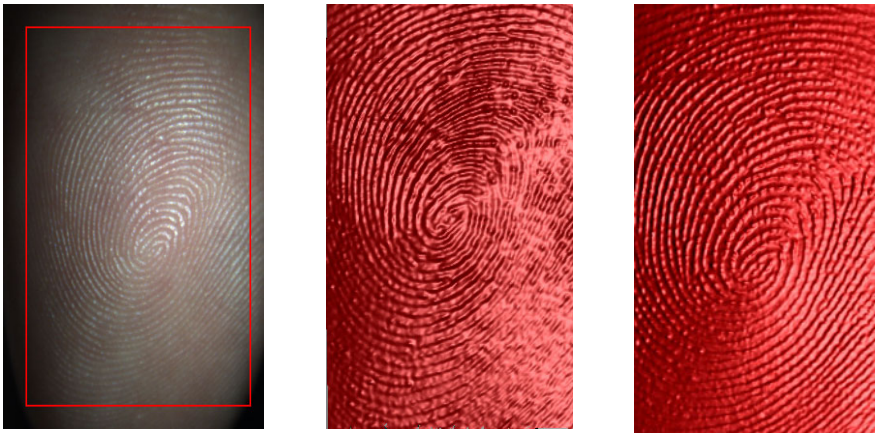

(a) (b) (c)

Fig. 7. (a) Finger image under one LED lighting. (b) Reconstruction result via traditional PS method which assumes a Lambert reflectance model. (c) Result by the proposed method.

5 Conclusion and Future Work

In this paper, we have proposed a novel photometric based system for the real-time 3D reconstruction of fingerprint. The system consists of only one camera and seven LED lamps. In the modeling of surface reflectance property, different with previous PS methods, we proposed a simplified HK model by using a Lambertion term to approximate the multiple scattering. A neutral network algorithm is used for accurate model parameters estimation. A calibration method is also proposed to determine the lighting directions as well as the correction of the lighting fields. Finally, to improve the visual effect of the reconstructed 3D model, a linear surface normal transformation is introduced. The experiments are conducted with a plasticine toy and human palm and finger to demonstrate its high performance. In comparison with traditional Lambertion based surface model, the proposed method can reconstruct the finger surface in finer details.

Future work can address the minimization of the whole hardware and the use of infrared LED lights so as to make the system more insensitive to ambient lights. We are also working on the 3D fingerprint processing algorithms and finally it will be

integrated with the hardware to accomplish a complete touch-less 3D fingerprint recognition system.

Acknowledgments

The work described in this article was partially supported by NSFC (Project no. 61002040) and Knowledge Innovation Program of the Chinese Academy of Sciences (Grant no. KGCX2-YW-156).

References

1. Delac, K., Grgic, M.: A Survey of Biometric Recognition Methods. In: 46th International Symposium in Electronics in Marine, pp. 184–193 (2004)
2. Chen, Y., Pariziale, G., Eva, D.S., Jain, A.K.: 3D Touchless Fingerprints: Compatibility with Legacy Rolled Images. In: Proceedings of Biometric, pp. 1–6 (2006)
3. Wang, Y.C., Daniel, L., Hassebrook, L.G.: Fit-Sphere Unwrapping and Performance Analysis of 3D Fingerprints. Applied Optics 49(4), 592–600 (2010)
4. Hanrahan, P., Krugeger, W.: Reflection from Layered Surfaces due to Subsurface Scattering. In: Proceedings of SIGGARPH, pp. 165–174 (1993)
5. Barsky, S., Petrou, M.: The 4-Source Photometric Stereo Technique for Three-Dimensional Surfaces in the Presence of Highlights and Shadows. IEEE Trans. on PAMI 25(10), 1239–1252 (2003)
6. Malzbender, T., Wilburn, B., Gelb, D., Ambrisco, B.: Surface Enhancement Using Real-time Photometric Stereo and Reflectance Transformation. In: Proceedings of the European Symposium on Rending, pp. 245–250 (2006)
7. Sun, J.A., Smith, M., Simth, L., Midha, S., Bamber, J.: Object Surface Recovery using a Multi-light Photometric Stereo Technique for Non-Lambertian Surfaces Subject to Shadows and Specularities. Image and Vision Computing 25(7), 1050–1057 (2007)
8. Osten, W.: A Simple and Efficient Optical 3D-Sensor based on Photometric Stereo. In: The 5th International Workshop on Automatic Processing of Fringe Patterns, pp. 702–706 (2005)
9. Georghiades, A.S.: Incorporating the Torrance and Sparrow Model of Reflectance in Uncalibrated Photometric Stereo. In: ICCV, vol. 2, pp. 591–597 (2003)
10. Belhumeur, P., Kriegman, D., Yuille, A.: The Bas-Relief Ambiguity. In: CVPR, pp. 1040–1046 (1997)
11. Zhao, H., Chen, K.Z.: Neural Network for Solving Systems of Nonlinear Equations. Acta Electronica Sinica 30(4) (2002)
12. Zhou, W., Kambhamettu, C.: Estimation of Illuminant Direction and Intensity of Multiple Light Sources. In: Heyden, A., et al. (eds.) ECCV 2002. LNCS, vol. 2353, pp. 206–220. Springer, Heidelberg (2002)
13. Zhang, Z.: A Flexible New Technique for Camera Calibration. IEEE Trans. on PAMI 22(11), 1330–1334 (2000)
14. Canny, J.: A Computational Approach to Edge Detection. IEEE Trans. on PAMI 8, 679–714 (1986)